

Article

GPR Imaging for Deeply Buried Objects: A Comparative Study Based on Compositing of Scanning Frequencies and a Chirp Excitation Function

Roger Tilley *, Hamid R. Sadjadpour and Farid Dowla

Department of Electrical Engineering, University of California, Santa Cruz, Santa Cruz, CA 95064, USA; hamid@soe.ucsc.edu (H.R.S.); dowla@soe.ucsc.edu (F.D.)

* Correspondence: rtvax@soe.ucsc.edu

Received: 13 February 2019; Accepted: 12 March 2019; Published: 18 March 2019



Abstract: Compositing of ground penetrating radar (GPR) scans of differing frequencies have been found to produce cleaner images at depth using the Gaussian mixture model (GMM) feature of the expectation-maximization (EM) algorithm. GPR scans at various heights (“Stand Off”), as well as ground-based scans, have been studied. In this paper, we compare the GPR response from a chirp excitation function-based radar with the response from the EM GMM algorithm compositing process, using the same mix of frequencies. A chirp excitation pulse was found to be effective in delineating the defined buried object, but the resulting image is less sharp than the GMM EM method.

Keywords: ground penetrating radar; expectation-maximization; Gaussian mixture model; maximum likelihood parameter estimation; finite-difference time-domain method; GprMax

1. Introduction

Methods to produce sharper delineated objects at depth using ground penetrating radar (GPR) is a continuing topic of study. Imaging results from ground-based scans and scans at various heights have benefited from the Gaussian mixture model (GMM) feature of the expectation-maximization (EM) algorithm technique [1–5] of combining scans at differing frequencies over the same terrain. It is well known that GPR scans at high frequencies better illuminate objects close to the surface with great fidelity and lower frequencies delineate objects at lower depths with less detail. We reported that combining scans at several frequencies “smartly” increased the resolution of objects at lower depths [1–5]. Scans were combined by using the GMM feature of the EM algorithm to sum weighted versions of each scan rather than just summing them together. We reported similar progress with GPR scans at various heights above ground [5]. There are areas that remain to be explored, such as better edge detection for buried objects and the use of other excitation functions with similar characteristics to the Ricker pulse used most often in GPR systems.

In this paper, we explore using a chirp excitation function-based radar to replace the multiple frequency scans used in the EM GMM algorithm analysis, comparing the result with EM processed scans. In Section 2, we discuss related work to combining GPR scans and processing scans with alternative excitation functions. In Section 3, we describe the EM data mixture process [6,7], briefly covering the maximum likelihood (ML) estimation process as it relates to the EM algorithm. In Section 4, we describe the chirp excitation function-based radar signal proposed for this analysis. In Section 5, we present results of the comparison of compositing simulated GPR scans at various frequencies with the result using a chirp excitation function-based radar signal, all computed using the GprMax [8] software program to develop the scan results. In Section 6, we draw conclusions and discuss future work.

2. Related Work

In the literature, chirp waveforms are mentioned in reference to synthetic aperture radar (SAR) [9–11] pulses and to a ground-based method called the vibroseis (seismic vibrator) technique [12–15]. Chirp waveforms are used in SAR systems to reduce the amount of power needed by the transmitter. Included among the benefits of using chirp waveforms is the size of the transmitter can be reduced allowing for smaller airborne radar systems. Implementing pulse compression techniques improves the signal to noise ratio. This, in conjunction with signal compression (correlation of received and transmitted signal), increases the range resolution and enhances object detection capability. Stolt [16], Gazdag [17], or FK(ω -k) migration [18,19] techniques were used to account for phase shifts due to the angles radar signals were sent and received from; they are not always the same.

Vibroseis [12–15] is a ground-based method consisting of low frequency vibrations generated by using a shaker or piston driven mass, creating a low-frequency chirp signal, often used for oil exploration. The vibroseis [12–15] method was developed and trademarked by Continental Oil Company (Conoco). Chirp signals from SAR and seismic vibration devices are processed in the same manner: cross-correlation of the reflections with the source signal determining wavelets representing target reflections. The use of a chirp waveform is our attempt to generate a response similar to the multiple frequency GPR scans combined by EM processing.

Our EM developed method, the compositing of GPR scans [1–5], was preceded by Dougherty et al. [20] who focused on a method to subtract the direct arrival pulse and combine each signal weighted with equal magnitudes. Booth et al. [21,22] followed Dougherty et al. [20] repeating their method but adding a frequency scan weighting technique using trace averaged amplitude spectra. Time invariant weighting methods were proposed by Booth et al. [21,22] matching compositing results to a least-squares idealized amplitude spectrum. Bancroft [23] introduced a method computing weights using one ramp to suppress a frequency's energy while using another ramp to increase a frequency's energy over time. Ramp start and stop times were determined by the wavelength of the frequency of interest. Bancroft also introduced weights based on the ratio of the average envelope of GPR frequencies used in the scans. Both methods, Booth et al. and Bancroft, provided minimal improvement over previous works. Our EM GMM method presented the best results of methods mentioned. The outcomes of these comparisons are detailed in references [3,4].

3. Expectation-Maximization Data Mixture Process

The EM algorithm is used to solve incomplete data problems [6,7], to determine membership weights of a collection of data points in a cluster, or to group like items in complex mixtures. Our expectation-maximization data mixture process exploits these features by defining a collection of data points in a cluster as a Gaussian mixture model (GMM) with membership weights. Then, using maximum likelihood (ML) parameter estimation to make the initial estimates of the unknown membership weights, establishing an ML estimation problem to solve. The EM algorithm reduces the ML estimation problem to a simpler optimization sub-problem which is guaranteed to converge.

We used the Gaussian mathematical distribution for the mixture model because it is often used when the distribution of the data is unknown. We define a finite mixture model as $f(x;\theta)$, of K mixture components of the following GMM function:

$$f(x;\theta) = \sum_{k=1}^K \alpha_k p_k(x | \theta_k), \quad (1)$$

where:

- $p_k(\underline{x}|\theta_k)$ are K mixture components with a distribution defined over $p(\underline{x}|\theta_k)$ with parameters $\theta_k = \{\underline{\mu}_k, C_k\}$ (mean, covariance)
- $p_k(\underline{x}|\theta_k) = \frac{1}{(2\pi)^{d/2} |C_k|^{1/2}} e^{-\frac{1}{2}(\underline{x}-\underline{\mu}_k)^T C_k^{-1}(\underline{x}-\underline{\mu}_k)}$ (2)
- α_k are K mixture weights, where $\sum_{k=1}^K \alpha_k = 1$
- $\{\underline{x}_1, \dots, \dots, \underline{x}_n\}$ Data set for a mixture component in d dimensional space.

The EM algorithm is an iterative process with two steps. The expectation step is the first step (E-step). The conditional expectation of the group of membership weights, (w_{ik} 's) for \underline{x}_i 's, are determined during this step. Unobservable data based on the mean and covariance matrix, θ_k , is integrated into the model. The maximization step (M-step) is the second step. In this step, new parameter values to maximize the finite mixture model are calculated: mixture weights, the mean, and covariance of the weights ($\alpha_k, \underline{\mu}_k, C_k$). The E-step and M-step are repeated until the GMM model converges, defined by a minimal change of the log-likelihood of the GMM function from one iteration to the next. The E-step and M-step are defined below:

E-Step

$$w_{ik} = \frac{p_k(\underline{x}_i|\theta_k) * \alpha_k}{\sum_{m=1}^K p_m(\underline{x}_i|\theta_m) * \alpha_m}, \text{ for } 1 \leq k \leq K, \quad 1 \leq i \leq N; \quad (3)$$

with constraint $\sum_{k=1}^K w_{ik} = 1$

M-Step

$$N_k = \sum_{i=1}^N w_{ik} \quad (4)$$

$$\alpha_k^{new} = \frac{N_k}{N}, \text{ for } 1 \leq k \leq K \quad (5)$$

$$\underline{\mu}_k^{new} = \left(\frac{1}{N_k}\right) \sum_{i=1}^N w_{ik} * \underline{x}_i, \text{ for } 1 \leq k \leq K \quad (6)$$

$$C_k^{new} = \left(\frac{1}{N_k}\right) \sum_{i=1}^N w_{ik} * (\underline{x}_i - \underline{\mu}_k^{new})(\underline{x}_i - \underline{\mu}_k^{new})^T \quad (7)$$

Convergence (log –likelihood of $f(\underline{x}; \theta)$) –

$$\text{Log}l(\theta) = \sum_{i=1}^N \log f(\underline{x}_i; \theta) = \sum_{i=1}^N \left(\log \sum_{k=1}^K \alpha_k p_k(\underline{x}_i|\theta_k)\right) \quad (8)$$

MATLAB programming language was used to implement these equations (MATLAB—a proprietary numerical programming language developed by The MathWorks, Inc. of Natick, MA., USA). In the GMM model, the variable ‘k’ represents the different scanning frequencies, and ‘x’ represents the GPR trace scans. Each GPR trace at a frequency transmitter (Tx), and receiver (Rx) position is analyzed and combined for all frequencies before moving on to the next position. The EM GMM processing steps are as follows.

EM GMM process:

1. Initialize algorithm parameters—weights (mixture and group membership), mean, covariance, for each trace.
2. E-Step—estimate parameters.
3. M-Step—maximize estimated parameters.
4. Check for convergence—log-likelihood of mixture model.
5. Repeat steps 2–4 until change from iteration to iteration is below or equal to a predefined value.
6. Combine traces with defined mixture weights.

The ML estimation process provides an estimate of an unknown parameter by determining the value that maximizes the probability of realizing the data we observed (likelihood). This process becomes hard when there are at least two sets of data and one is partially observed or hidden and the

mixture parameters are to be estimated. For the case where there is only one unknown parameter, the ML estimation process can be described as follows. Given a random sample X_1, X_2, \dots, X_n , independent and identically distributed (i.i.d.), with a probability density function (PDF) of $f(x_i, \theta)$ with an unknown parameter, θ , to be estimated, the joint PDF can be labeled $L(\theta)$.

$$L(\theta) = P(X_1 = x_1, X_2 = x_2, \dots, X_n = x_n) = f(x_1; \theta) * f(x_2; \theta) \dots f(x_n; \theta) = \prod_{i=1}^n f(x_i; \theta) \quad (9)$$

Describing the random sample as Gaussian with known variance, σ^2 , and unknown mean, μ , then the likelihood equation converts to the following:

$$L(\mu) = \prod_{i=1}^n f(x_i; \mu, \sigma^2) = \sigma^{-n} (2\pi)^{-n/2} \exp\left(-\frac{1}{2\sigma^2} \sum_{i=1}^n (x_i - \mu)^2\right) \quad (10)$$

To determine the value of the parameter μ , which maximizes the likelihood equation, take the partial derivative of the log-likelihood equation with respect to (w.r.t.), the mean, μ , set the resultant equation equal to 0, and solve for the variable μ . To verify that a value, μ , that maximizes the likelihood equation has been found, take the second partial derivative of the log-likelihood equation w.r.t. μ . Should the result be a negative value, this confirms a maximum value, μ , has been found as demonstrated by the following equations.

$$\text{Log}(L(\mu)) = -n \log(\sigma) - \frac{n}{2} \log(2\pi) - \sum_{i=1}^n \frac{(x_i - \mu)^2}{2\sigma^2} \quad (11)$$

$$\frac{\partial}{\partial \mu} (\log(L(u))) = -2(-1) \sum_{i=1}^n \frac{(x_i - \mu)}{2\sigma^2} = 0 \quad (12)$$

$$\text{Solve for } \mu; \mu = \frac{\sum_{i=1}^n x_i}{n} \quad (13)$$

$$\begin{aligned} &\text{Second derivative} \\ \frac{\partial^2}{\partial \mu^2} (\log(L(u))) &= \sum_{i=1}^n \frac{(-1)}{\sigma^2} = -\frac{n}{\sigma^2} \end{aligned} \quad (14)$$

For a distribution of mixture parameters to be estimated, of the form $f(x) = \sum_{k=1}^K \alpha_k f(x; \theta_k)$, where there are K number of components in the mixture model and for each K there is a PDF, $f(x; \theta_k)$, with weights α_k , an observed data set x , and constraints $\sum_k \alpha_k = 1$ and $\alpha_k \geq 0$ for all k , the resultant joint PDF (likelihood equation) takes the form with n observed data points for each k as follows:

$$L(x|\alpha, \theta_k) = \prod_{i=1}^n \sum_{k=1}^K \alpha_k f(x_i; \theta_k) \quad (15)$$

The log of the likelihood equation—

$$\text{Log}((L(x|\alpha, \theta_k))) = \sum_{i=1}^n \log \sum_{k=1}^K \alpha_k f(x_i; \theta_k) \quad (16)$$

Solving this equation using the ML estimation process requires determining the derivative of the log of sums and a start weight value, α_k , which presents a challenge. Many local maxima can be found that are less than the global maximum using a created weight value, α_k . Selecting the weight value which attains the global maximum is unlikely in short order. The EM algorithm process method estimates the weights and guarantees convergence of the log-likelihood equation [6,7] to a non-decreasing local maximum with each iteration outlined in the EM GMM process steps. A global maximum is eventually reached. The ML estimation optimization process is reduced to a sequence of simpler optimization sub-problems, each guaranteed to converge. The E-step calculates the probability of the weight parameter values first, using defined initial parameter values, and later, using parameter values calculated by the M-step process. The M-step recalculates the model parameters, then calculates the maxima for that set of parameters based on the ML estimation process.

For compositing of GPR frequency scans, the weights of each frequency are unknown (hidden). The EM algorithm method of accomplishing solutions to problems with hidden or incomplete data [6] is distinctly different than other optimization problem solvers, making it the featured candidate for combining multiple GPR frequency scans.

4. Chirp Excitation Function-Based Radar Signal

A signal in which the frequency increases with time or decreases with time is often named a chirp or sweep signal after the sound often made by birds. Creating a chirp excitation function-based radar signal, for use in this study, required computing a nominal chirp signal and deciding among several attributes. Increasing or decreasing chirp, exponential or linear, length of time the chirp signal is applied, the start time the chirp signal is applied, and the magnitude, are a few of the attributes requiring definition. For our study we chose an increasing linear chirp with a maximum amplitude of 1. Increasing linearly, in that the change from one frequency to the next frequency increases in a linear fashion.

For use in the GprMax software program, we created sampled chirp signals structured to match each time step for the delta area (Δx and Δy) of a 2-D analysis. We arbitrarily chose the length of time the chirp signal would be applied (*view_width*) as $\frac{1}{4}$ of the entire time the computer analysis was defined to run (*tmax*). The length of time was similar to that when a Ricker pulse signal is used in GPR analyses. The chirp start time was defined arbitrarily as 10 time samples. We implemented an added feature of using a Hanning window to soften the initial start and end of the created chirp pulse.

These choices were compiled and implemented in MATLAB code. Figure 1, shows the code used and Figure 2 shows the labeled result. The increasing linear chirp signal was designed to cover the frequencies used in the current EM analysis (20, 30, 50, 100, 500, and 900 MHz); consequently, the linearly increasing chirp start and end frequencies were defined as 20 MHz and 900 MHz, respectively. The frequency time step is not explicitly shown in the computer code of Figure 1 but can be calculated using the following equation based on the variables defined in Figures 1 and 2.

$$\text{frequency step} = df = \left(\frac{f2 - f1}{\text{sweep time}} \right) * \text{time step} \quad (17)$$

where:

$f1$ —chirp start frequency

$f2$ —chirp end frequency

$\text{sweep time} = t_{\text{max}} / \text{view_width}$

$$\text{time step} = dt = \frac{1}{\left(c * \sqrt{\left(\frac{1}{\Delta x} \right)^2 + \left(\frac{1}{\Delta y} \right)^2} \right)} (\text{GprMax magic time step}) \quad (18)$$

c = speed of light (3×10^8 m/s),

$(\Delta x, \Delta y)$ —2-D analysis defined delta area.

For the parameters defined in Figure 2, the frequency step is 0.234 MHz. This value varies with the modeling area definition. The computer code is structured using the MATLAB standard routine “Chirp” to generate a basic chirp signal and the MATLAB routine “Hanning” to generate a Hanning window.

```

function [x1] = rdr_chirp_file_all(tmax,dx,dy,f1,f2,nstart,view_width)
%GprMax excitation file generator.
%generates an excitation file stored as ascii magnitude values
%per time step.
%
%dx - delta x of area to scan
%dy - delta y of area to scan
%dt - magic time step - dt = 1/(c*(sqrt((1/dx)^2 + (1/dy)^2))
%f1 - starting chirp frequency
%f2 - ending chirp frequency
%time - time step vector
%nstart - number of start points from 0
%view_width - view of signal pulse (default 2)
%tmax - maximum scan time
%nt - number of time steps -- round(tmax/dt)
%
%x1 - output signal
%filenm - file name of stored ascii file of data
%-----

dt1 = (1/dx)*(1/dx);
dt2 = (1/dy)*(1/dy);
dt3 = sqrt(dt1 + dt2);
dt = 1/(3.00e8 * dt3); %magic time step
nt = round(tmax/dt);
time = [0:dt:nt*dt];
nstart = nstart; view_width = view_width;

ch = chirp(time,f1,tmax/view_width,f2);
s1 = ch(1:round(length(time)/view_width));
s1 = s1.*hanning(length(s1));
x1 = zeros(size(time));
x1(nstart:nstart+length(s1)-1) = s1;

filenm = strcat('excite_chirp','_',num2str(tmax*1e9),'e-9','_', ...
    num2str(dx),'_',num2str(dy),'_', num2str(f1/1e6),'e6', ...
    '_',num2str(f2/1e6),'e6','_','.dat');
save (filenm, 'x1', '-ascii', '-double');

```

Figure 1. Chirp signal MATLAB code.

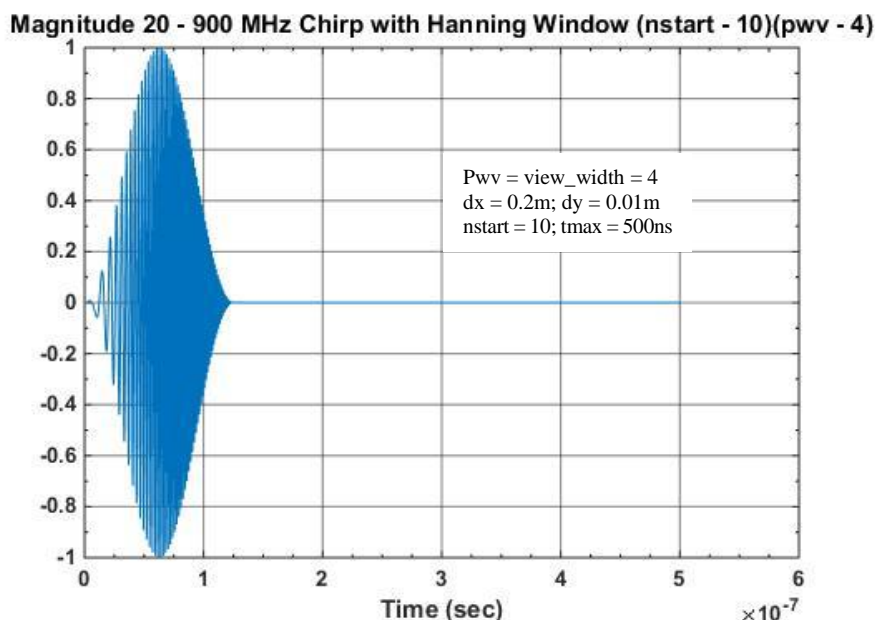


Figure 2. Computed chirp signal.

5. Results

To determine the capability of the chirp excitation function scans to replace the combination of individual frequency scans, using the EM GMM method, we ran the same analyses on three fictional areas with a chirp excitation signal instead of the frequency scans with six different frequencies.

The original scans used frequencies 20, 30, 50, 100, 500, and 900 MHz, combined using the EM GMM method. The chirp signal used was a linearly increasing chirp from 20 MHz to 900 MHz, processed through a Hanning window, as shown in Section 4, Figure 2. The frequency step is not directly calculated by the MATLAB chirp routine but can be calculated using Equations (17) and (18). The frequency step varies with the length of time (tmax) the scan is active and the delta model area (Δx , Δy). Simulation model areas were defined using the modeling software package GprMax by Giannopoulos [8] via the finite-difference time-domain (FDTD) analysis method solution to Maxwell's electromagnetic wave propagation equations for GPR. As previously reported [1–5], only 2-D analyses were performed. However, the software is capable of 3-D analysis as well. We reported earlier [1,4] the concurrence between actual scan results and simulated scan results; a brief review is included in Appendix A.1. Appendix A.2 includes a brief review of a test case of the EM GMM process operation [2,4]. Examples were constructed to allow for various transmitter (Tx) and receiver (Rx) heights above ground for two different target types to be studied. Tx/Rx were always positioned at the equal heights, above ground, for each scan. Heights included 5, 10, 20, and 40 m. A total of three modeling areas were previously defined and re-examined here for comparison of the EM GMM method with the chirp excitation function method. The removal of the direct arrival and ground bounce signals allows for a better focus on the reflections from the buried targets. Removal of these signals is easily done in simulation. We remove these signals from the analysis by scanning with the target(s) in place first, then without the target(s) in place. We simply subtract the two results to achieve removal. The result is scaled to a max value of 1 and processed. The magnitude of each processed signal plotted is scaled to a value of 1. Our interest in constructing the modeling spaces, defined below, was to evaluate the responses at defined distances above ground in an air medium, simulating the use of an unmanned vehicle performing the GPR scans, attempting to reliably image unknown buried objects.

5.1. Defined Simulated Analysis Space 1

One defined area modeled consisted of a Tx/Rx positioned 5 m above the ground in air. The target is a perfect electrical conductor buried 10 m below the surface in a moist sand medium. Moist sand has a relative permittivity (ϵ_r) of 9.0 and an electrical conductivity of 0.001 mS/m, where the velocity through the media is 0.1 m/ns. Free space or air has a relative permittivity of 1.0 and is considered “lossless” with an electrical conductivity of 0, where the velocity through the media is 0.3 m/ns. The defined space is labeled Simulated Analysis 1 (SA1). The target is 2 m in length and 0.5 m in depth. The model area is 10 m in width and 25 m in depth. The Tx/Rx pair was moved along the scan axis (x-axis) 0.25 m per step for a total of 36 scans. The Tx starts at 0.5 m ending at 9.5 m in the x direction. The Rx starts at 0.75 m ending at 9.75 m in the x direction. Each scan, at 425 ns in length, is long enough to receive a reflected signal from 24 m below the Tx/Rx pair in a combined medium of air and moist sand. SA1 has a grid space of 200 points in the x direction, (Δx —0.05 m), and 500 points in the y direction, (Δy —0.05 m). Figure 3a [2–5] shows the model, Tx/Rx positions, and the target area. Figure 3b [2,4,5] shows the six signals combined by scaling each signal's max value to the same magnitude with the direct arrival and ground bounce removed. The target reflection covers a broad area in depth from 240 ns to 320 ns (two-way travel time), a rough indication of the target depth. The two-way travel time reflects the increased length in signal travel, above the vertical distance, due to the ray refraction caused by dissimilar medium, air to moist sand, resolvable using Snell-Descartes law of refraction.

Figure 4a [2–5] shows the result from combining six different frequencies using the EM GMM method to determine the weight associated with each signal to be combined. The target is correctly shown approximately 15 m below Tx/Rx pair (240 ns), 10 m below ground. Figure 4b shows the analysis result from the chirp excitation signal. The chirp result is not as broad as Figure 3b [2–5] but it still more uncertain than Figure 4a [2–5] with the same not well-defined edge detection of the target.

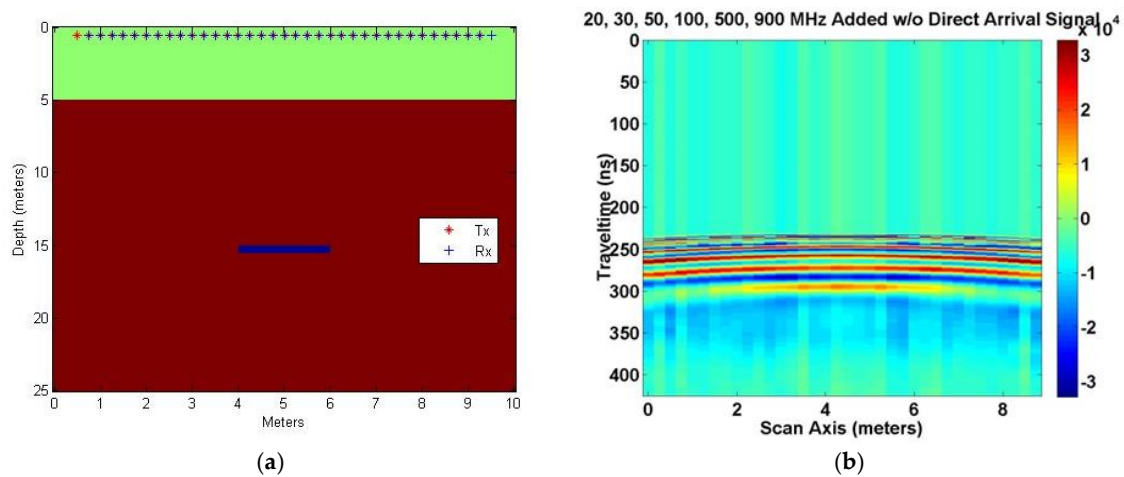


Figure 3. (a) Defined space with buried target at 15 m depth with transmitter/receiver (Tx/Rx) pair 5 m above ground [2–5]; (b) Sum of frequency signals with direct arrival and ground bounce signals removed [2,4,5].

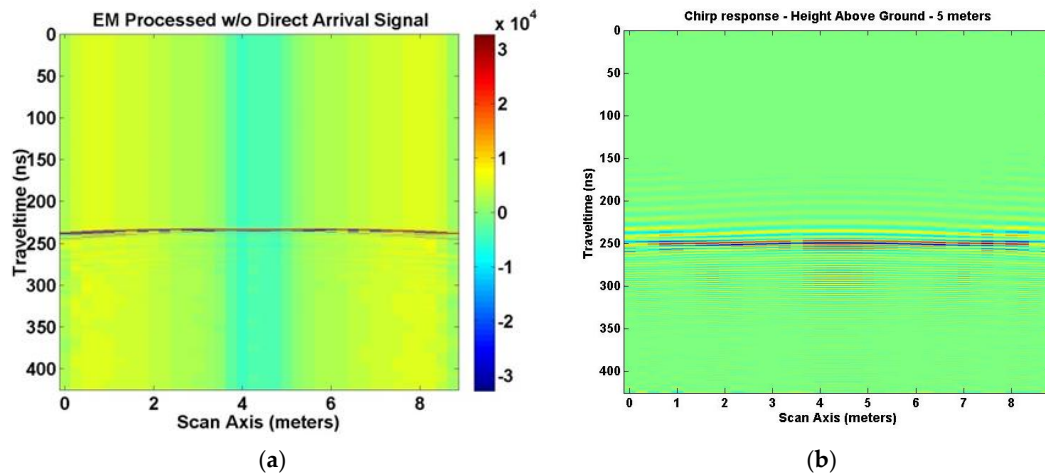


Figure 4. (a) Expectation-maximization (EM) sum of frequency signals with direct arrival and ground bounce signals removed [2–5]. (b) Chirp excitation signal response with direct arrival and ground bounce signals removed.

Though model SA1 has an area twice as deep as it has in width (bore hole), the analysis result is still valid and points to real differences in the techniques, EM GMM verses chirp excitation. A bore hole can be described as a very narrow width scanning area. The significance of the width is that the area scanned may not be wide enough to show the entire hyperbola, which normally forms above and around the object being scanned. This is occurring in Figure 4. Adding to the problem is that hyperbola formation is affected by the length of the object and the depth. With the increase in depth and object length, the hyperbola tends to flatten out. Heights of 10, 20, and 40 m above ground with the same model SA1 features were examined to determine what other information, if any, might be realized. Figures 5 and 6 show and compare the 1-D plots of individual traces for the EM GMM analysis and chirp excitation analysis results at 5 m above ground. Figure 5a shows the trace (18) at 5 m out of 10 m total in the x direction, roughly over the target for the EM GMM process. Figure 5b depicts the same x direction trace for the chirp excitation analysis. The chirp trace is extended in time which is reflected in the multiple hyperbolas and target “ghosting” appearing in the image plot.

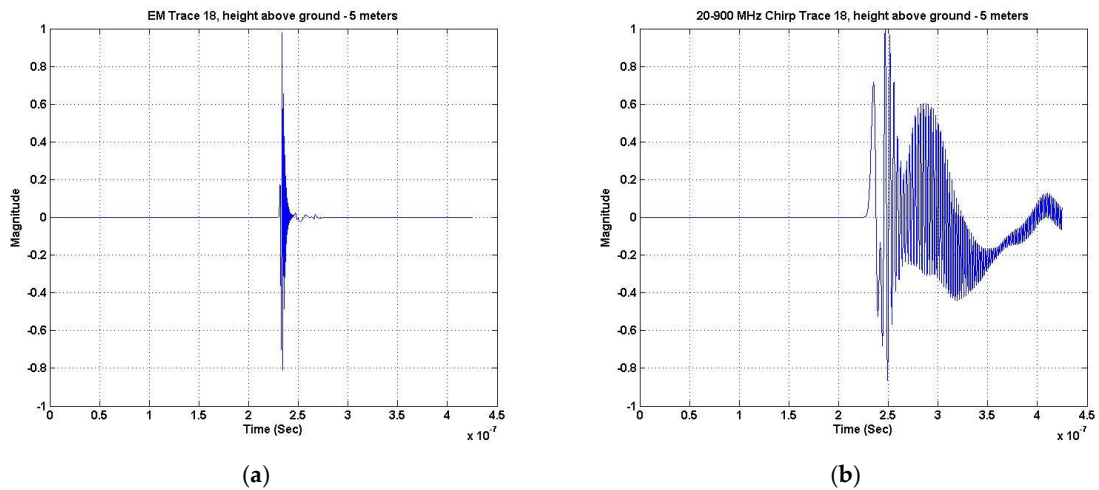


Figure 5. (a) Trace 18 of 36 traces total, roughly 5 m out of 10 m total distance in x direction, a 1-D plot of EM Gaussian mixture model (GMM) analysis. (b) Trace 18 of 36 traces total, roughly 5 m out of 10 m total distance in x direction, a 1-D plot of chirp excitation analysis.

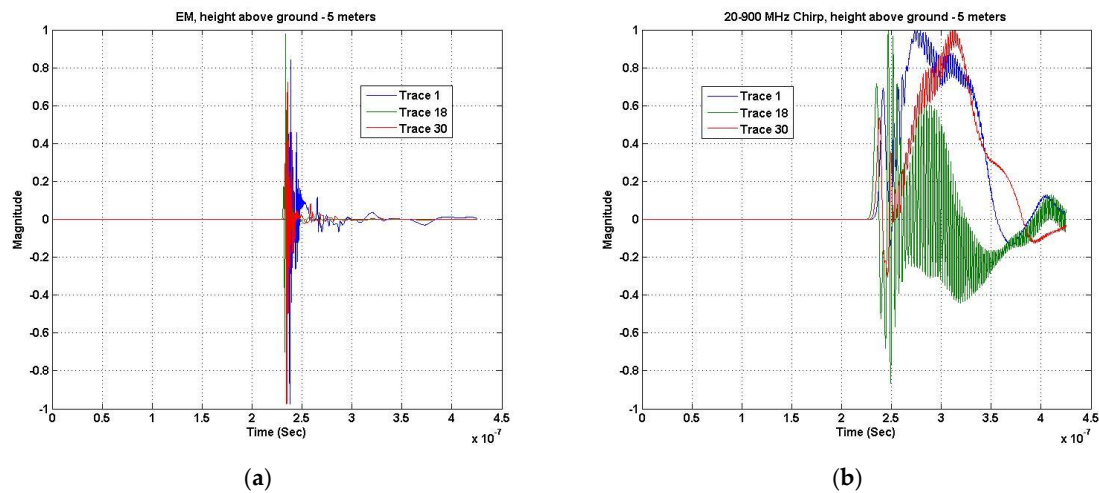


Figure 6. (a) Traces 1, 18, and 30; plots of EM GMM analysis. (b) Traces 1, 18 and 30; plots of chirp excitation analysis.

Figure 6 depicts traces at approximately 0.3 m (trace 1), 5 m (trace 18), and 8.3 m (trace 30). The EM GMM method produces a much tighter trace spread over the width of the scanned area (Figure 6a). The chirp excitation response is noticeably broader (Figure 6b). However, they both indicate a 240 ns two-way travel time, corresponding to a target at 15 m below the Tx/Rx pair. Of note is that the direct arrival and ground bounce signals have been removed.

Figures 7 and 8 [5] depict the changes to the SA1 defined space model and the GPR analysis result at 10 m in height above ground, respectively. The reflected GPR response shows the target at 20 m below the Tx and Rx for a two-way travel time of 270 ns. The chirp response (Figure 8b) is not as well defined in depth and the width suffers from the bore hole effect.

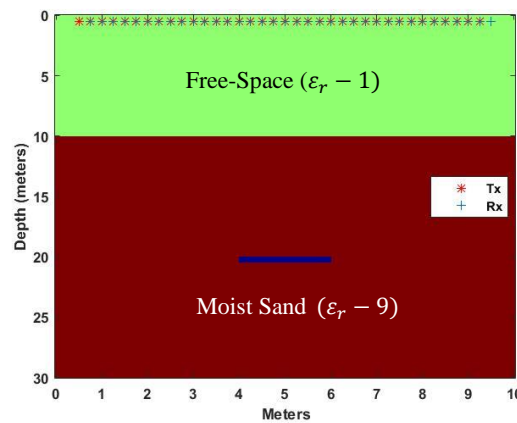


Figure 7. Defined space SA1, with buried target at 20 m depth from Tx/Rx pair, 10 m above ground [5].

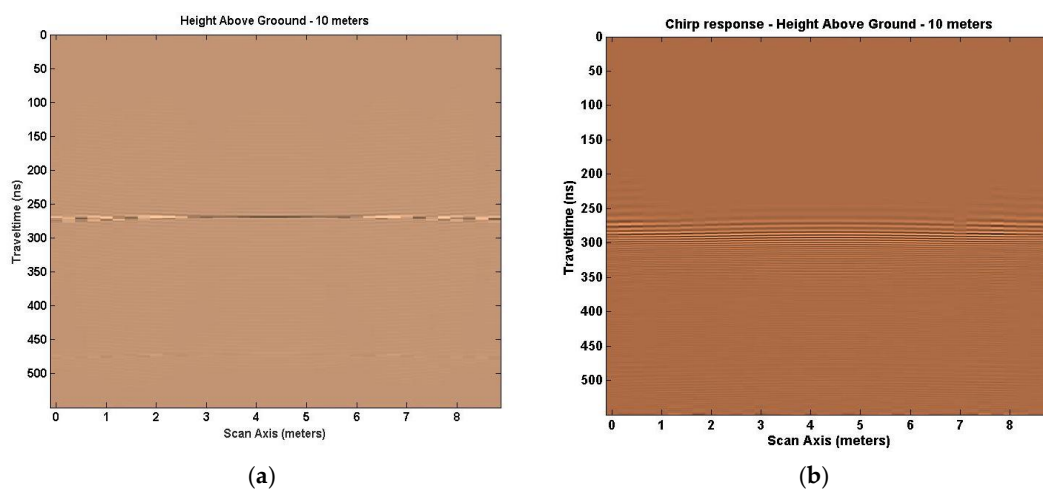


Figure 8. (a) Output response of SA1, EM sum of frequency signals with direct arrival and ground bounce signals removed [5]. (b) Chirp excitation signal response with the direct arrival and ground bounce signals removed.

To compensate for geometric distortion of chirp waveform responses, we looked at using three methods: the phase shift migration method of Gazdag [17], signal compression (correlation of received signal with transmitted signal), and filtering the received signal into six separate frequencies (the frequencies used in the EM GMM analysis), then using the result to calculate a EM GMM response. The Gazdag method [17], like the Stolt [16] and FK [18,19] techniques, attempt to account for phase shifts that occur when the angles the radar signals are sent from are different than the angle the signals are received. The change from the unprocessed chirp response to a Gazdag [17] processed chirp signal is minimal but important. The signal echoes above the reflected target are reduced. Much was not expected because our transmit and receive angles do not change very much, especially for 2-D, so there is no azimuth correction to make. Figure 9a depicts the response due to Gazdag [17] for Tx/Rx pairs at 5 m in height above ground, and Figure 9b depicts the response at 10 m in height above ground.

Figure 10 shows the result of correlating (cross-correlation) the transmitted signal with the received signal for Tx/Rx pairs at 5 m and 10 m above ground. Signal to noise enhancement is defined as the result. Multiple lines above the reflected target position are significantly reduced or non-existent, displaying an output closer to the EM GMM method response. Good edge detection and broadness in depth of the response is still less than desired.

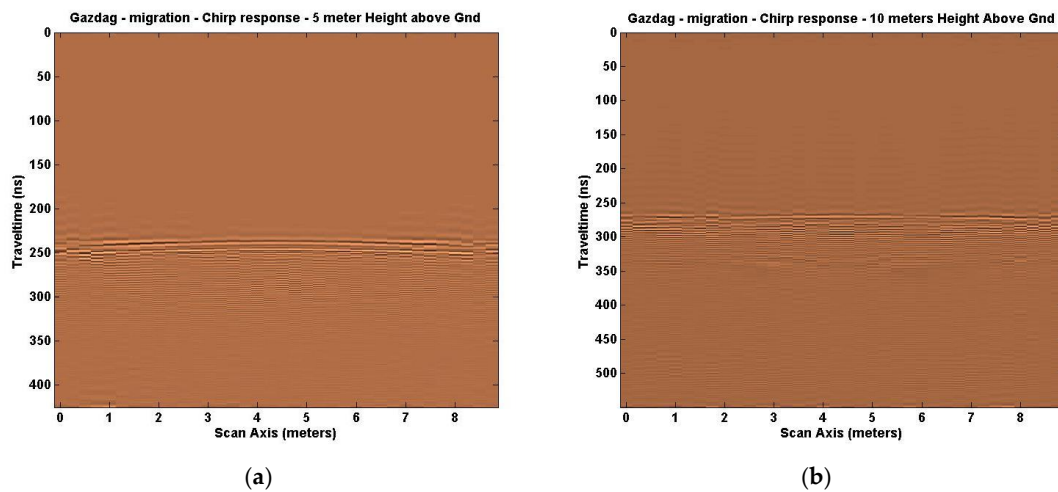


Figure 9. (a) Gazdag [17] translated output response of SA1 for 5-m height chirp excitation. (b) Gazdag [17] translated output response of SA1 for 10-m height chirp excitation.

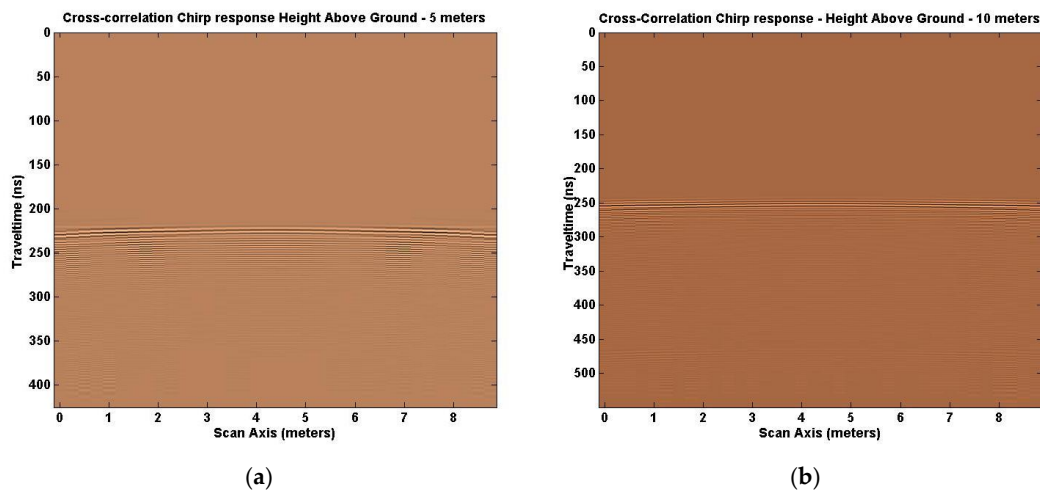


Figure 10. (a) Cross-correlation of chirp excitation response of SA1 model at 5-m height above ground. (b) Cross-correlation of chirp excitation response of SA1 model at 10-m height above ground.

Figure 11 shows the result of filtering the original chirp excitation response with six different filters: a 20 MHz low pass filter, 30 MHz bandpass filter, 50 MHz bandpass filter, 100 MHz bandpass filter, 500 MHz bandpass filter, and a 900 MHz high pass filter to mimic the 6 frequencies used for the compositing process. Each section began with unit amplitude, then underwent the EM GMM process to determine the weights needed to combine these six frequency responses. The result was not as impressive as we would have liked. A multi-band reflection remained in the solution shown for Tx/Rx pairs at 5 m and 10 m above ground.

Further comparison results for Tx/Rx pair heights at 20 and 40 m were not included in this paper because no further conclusions were realized beyond the normal signal degradation as the target depth increased. Geometric distortion methods for this model space (SA1) were no longer considered for study, based on the above results.

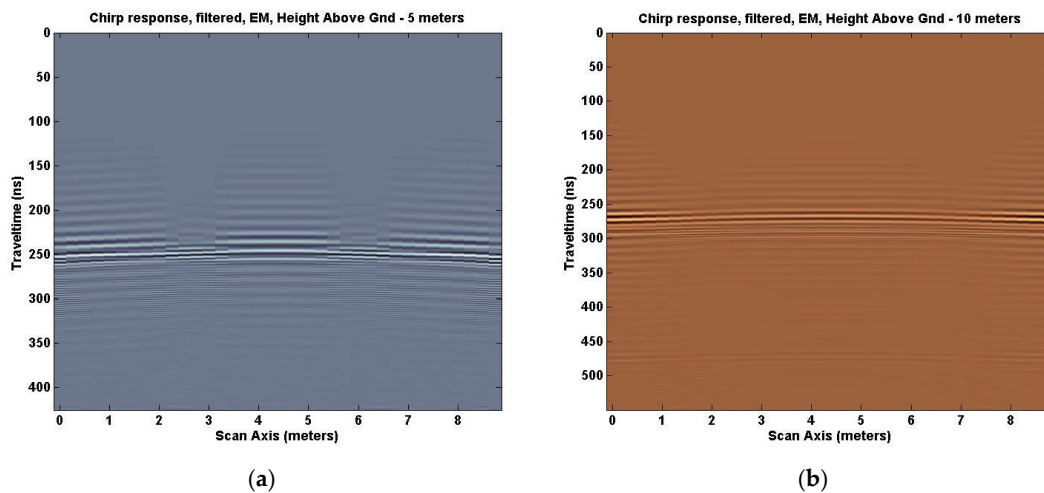


Figure 11. (a) SA1 model Chirp response, Tx/Rx at 5 m, filtered into 6 frequencies, 20, 30, 50, 100, 500, and 900 MHz, then processed with the EM GMM algorithm. (b) SA1 model Chirp response, Tx/Rx at 10 m, filtered into 6 frequencies, 20, 30, 50, 100, 500, and 900 MHz, then processed with the EM GMM algorithm.

5.2. Defined Simulated Analysis Space 2

A more complicated set of targets were developed for follow-on analyses. The second defined space model developed (Simulated Analysis 2—SA2) consisted of an area 30 m in width and 25 m in depth with almost no space above ground (0.15 m) for the Tx/Rx pair. Eight targets were buried at eight different levels. These targets represent sheets of corrugated aluminum, modeled as perfect electrical conductors. Each sheet was approximately 2 m in length and 0.1 m in depth. The eight burial levels were 4.565, 6.065, 8.565, 10.065, 12.815, 14.065, 16.565, and 18.065 m. The odd metric values are due to a not well-defined start burial level of approximately 15 ft deep (4.565 m). Each additional increase in depth was computed in meters (1.5, 2.5, 1.5 m, etc.). The sheets were buried in dry sand with a relative permittivity (ϵ_r) of 3.0 and electrical conductivity of 0.001 mS/m, with a velocity through the medium of 0.1732 m/ns. The Tx/Rx pairs were swept along the scan axis with the Tx starting at 0.5 m and ending at 24.85 m. The spacing between a Tx and Rx remained at 0.25 m. Each scan is 550 ns long and capable of receiving a reflected signal from roughly 48 m below each Tx/Rx pair in dry sand. The model grid space is 150 points in the x direction (scan axis: $\Delta x=0.2$ m) and 2500 points in the y direction (depth axis: $\Delta y=0.05$ m). Scanning frequencies for the EM GMM response are the same as before (Section 5.1). The chirp excitation function and frequency step changed as calculated using the software program in Figure 1 and Equations (17) and (18), respectively, detailed in Section 4. The direct arrival and ground bounce signals were removed as before (Section 5.1).

The model SA2 is shown in Figure 12. The result from the EM GMM method, shown in Figure 13a, correctly depicts the depths of the sheet targets at approximately 50, 70, 100, 116, 148, 160, 190, and 208 ns for two-way travel time. Figure 13b depicts the chirp excitation function response and shows better edge detection capability, while Figure 13a shows better depth delineation. The same result was found previously in the model SA1 studies.

We repeated the analysis for a Tx/Rx pair at a height of 5 m above ground in free space. Figure 14 shows the SA2 model used for the analysis. Figure 15a shows the response with the EM GMM method, and Figure 15b shows the chirp excitation signal response. Again, the chirp signal response displays good edge detection but coarse depth detection. Each method detects eight objects but not clearly. The chirp result shows eight “ghost” reflections underneath eight objects.

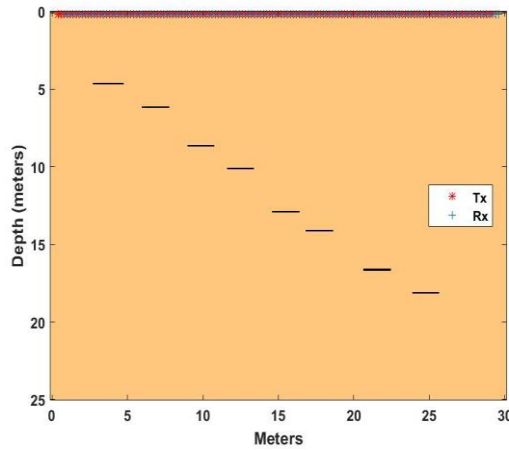


Figure 12. Defined space SA2, with (8) 2-m-long plates, 0.1 m thick at nearly 5, 6, 9, 10, 13, 14, 17, and 18 m with Tx/Rx pair 0.15 m above the ground [2–4].

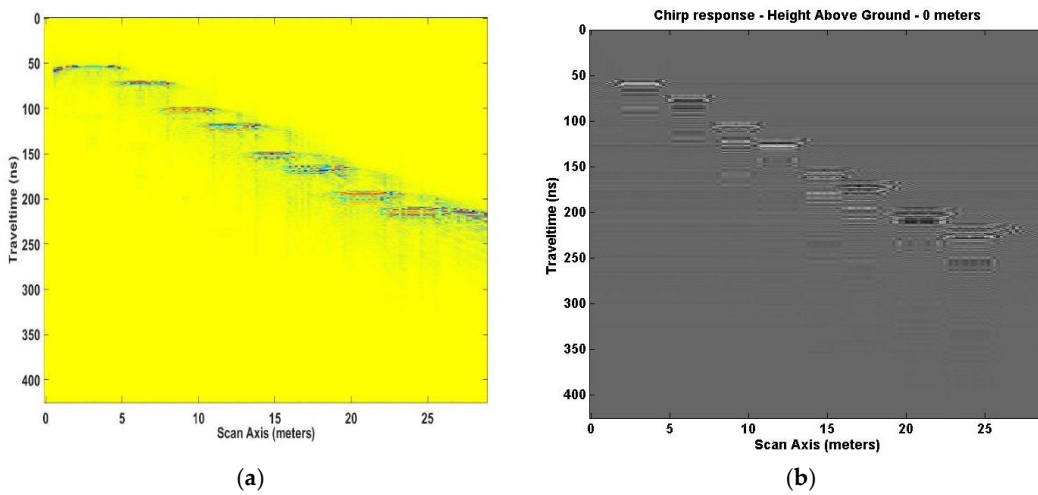


Figure 13. (a) Output response of SA2 model, EM sum of frequency signals with direct arrival and ground bounce signals removed [2–4]. (b) Output response of SA2 model, chimp excitation function with the direct arrival and ground bounce signals removed.

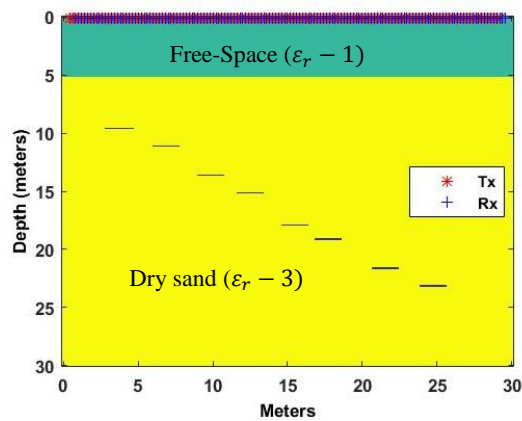


Figure 14. Defined space SA2, with (8) 2-m-long plates, 0.1 m thick at nearly 5, 6, 9, 10, 13, 14, 17, and 18 m with Tx/Rx pair 5 m above ground [5].

We repeated a look at compensation methods for geometric distortion of chimp waveform responses that we explored in Section 5.1., i.e., Gazdag migration [17], correlation, and separating the

response by filtering with six separate filters then compositing the result using EM GMM. Figure 16 shows the Gazdag [17] result for a Tx/Rx pair at approximately 0 m (0.15) and 5 m height above ground. Except for the more noticeable “ghosting” below each recognized target, the change from Figure 15b is barely noticeable in Figure 16. Figure 17 shows the result after correlating the transmitted signal with the received chirp signal with a Tx/Rx pair at approximately 0 m (0.15) and 5 m. With migration the output is a bit more cluttered, and with correlation much more clutter is evident. In Figure 17, about all that can be determined is that there are objects proceeding in a downward stair-step fashion as one moves along the x axis (scan axis) with at least eight concentrated reflections underneath at least eight objects.

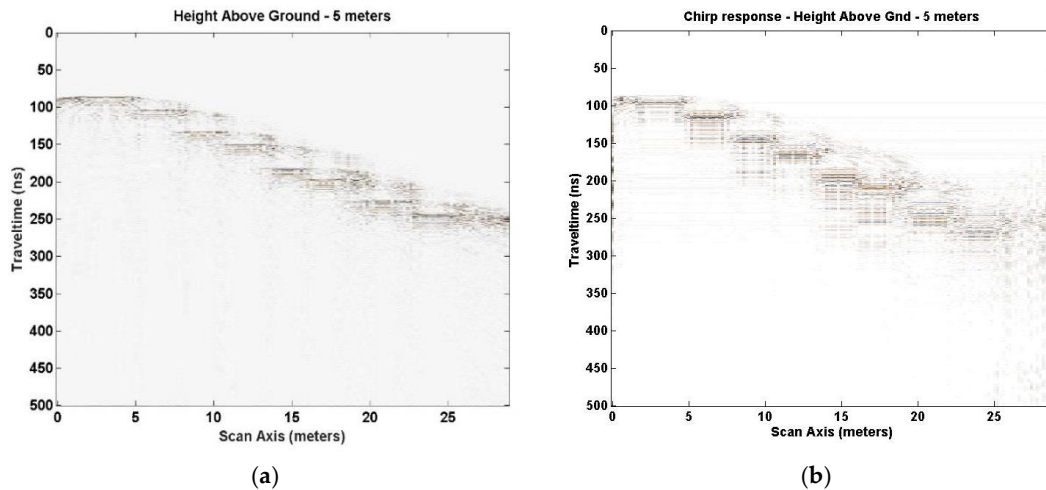


Figure 15. (a) Output response of SA2, EM sum of frequency signals with direct arrival and ground bounce signals removed [5]. (b) Output response of SA2 model, chirp excitation function with the direct arrival and ground bounce signals removed.

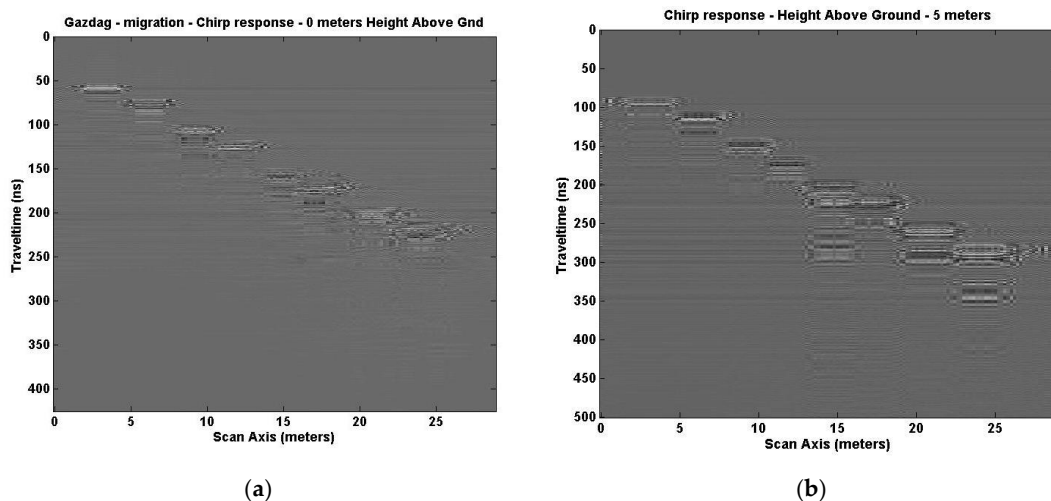


Figure 16. (a) Gazdag [17] translated SA2 model output from chirp excitation with Tx/Rx at 0.15 m. (b) Gazdag [17] translated SA2 model output from chirp excitation with Tx/Rx pair at 5 m.

Filtering the original chirp excitation response into six separate frequencies then using the EM GMM process to combine them is shown in Figure 18 at heights of approximately 0 m (0.15) and 5 m for a Tx/Rx pair. There is very little change in response of the chirp excitation images using this filtering technique, certainly not enough to routinely apply this feature to the data received. The multiband reflection at each target object remains and is possibly enhanced making the image a bit less clear. The results are similar to the SA1 model case of Section 5.1. EM GMM scanning comparison results

with chirp excitation responses for Tx/Rx heights of 10, 20, and 40 m do not appear in this paper because no further conclusions were realized beyond the normal signal degradation as the target depth increased.

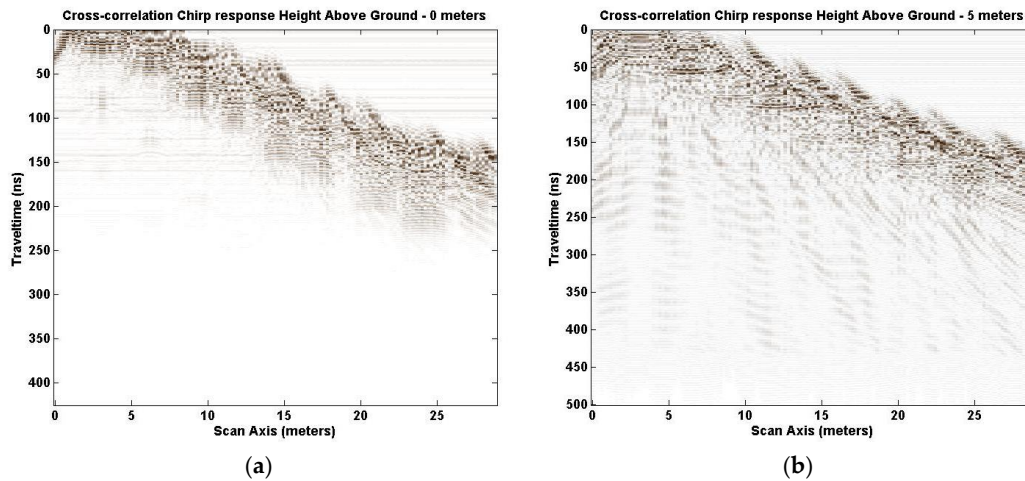


Figure 17. (a) Cross-correlation of chirp excitation response of SA2 model for Tx/Rx pair at 0 m above ground. (b) Cross-correlation of chirp excitation response of SA2 model for Tx/Rx pair at 5 m above ground.

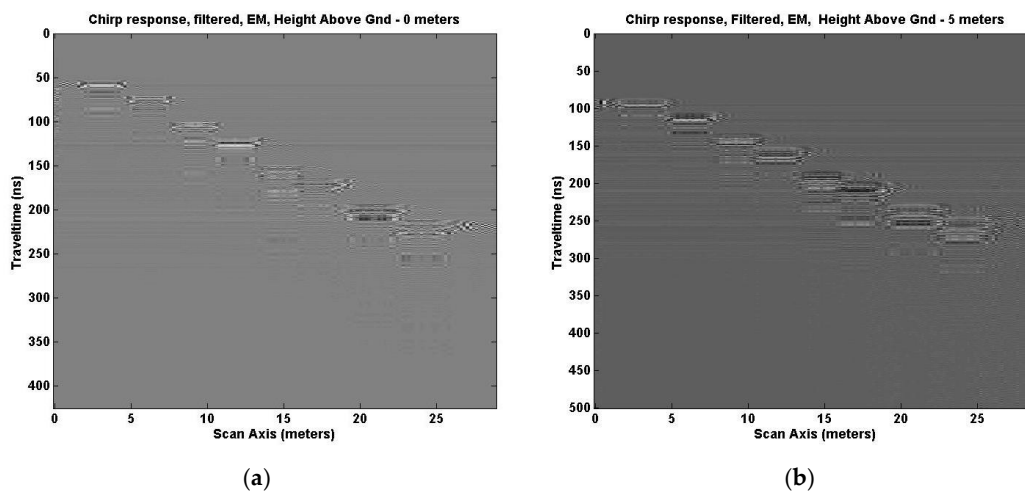


Figure 18. (a) SA2 model Chirp response with Tx/Rx pair at 0.15 m in height, filtered into 6 frequencies, 20, 30, 50, 100, 500, and 900 MHz, combined using EM GMM. (b) SA2 model chirp response with Tx/Rx pair at 5 m in height, filtered into 6 frequencies, 20, 30, 50, 100, 500, and 900 MHz, combined using EM GMM.

5.3. Defined Simulated Analysis Space 3

We developed a third defined space model labeled SA3 (Simulated Analysis 3) using the same area dimensions and target designations of the SA2. The SA3 model placed the target objects in non-homogenous materials instead of the homogenous materials used in SA1 (moist sand) and SA2 (dry sand). A model area was created with dry sand, clay, concrete, granite, and limestone with a relative permittivity (ϵ_r) of 3.0, 5.0, 6.0, 4.0, and 7.0, respectively, noted in Figure 19. The velocity through each medium is 0.1732 m/ns (dry-sand), 0.1342 m/ns (clay), 0.1225 m/ns (concrete), 0.1500 m/ns (granite), and 0.1134 m/ns (limestone). In Figure 19 there are coloration differences to denote the different media used in the model. As before, the EM GMM response is observed side by side to the chirp excitation function response and the same frequencies are used in the analysis.

The study was conducted for Tx/Rx heights of 5, 10, 20, and 40 m above ground, however, responses at 10, 20, and 40 m are not included or discussed in this paper; no new information is realized beyond signal degradation as target depth increases. Figure 19 depicts the SA3 model with Tx/Rx pairs 5 m above ground. Figure 20a shows the EM GMM response, while Figure 20b depicts the chirp excitation function response. The results are similar to those discussed earlier among the SA2 model results. Figure 20a continues to have the edge detection problem with minor reflections under each of the eight objects. Figure 20b continues to show better edge detection but much larger reflections under each of the eight objects, some large enough to be considered objects in themselves and not “ghost” reflections. Again, no further conclusions are realized over the SA2 model cases except for the signal loss due to the different media of the SA3 model. Results of scans at 10, 20, and 40 m were not included in this paper because new findings have not been identified besides the normal signal degradation that occurs as the buried target depth increases.

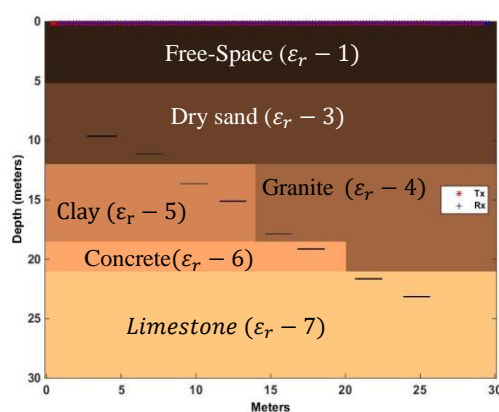


Figure 19. Defined space of SA3, (8) 2-m-long plates, 0.1 m thick with Tx/Rx pair 5 m above ground [5].

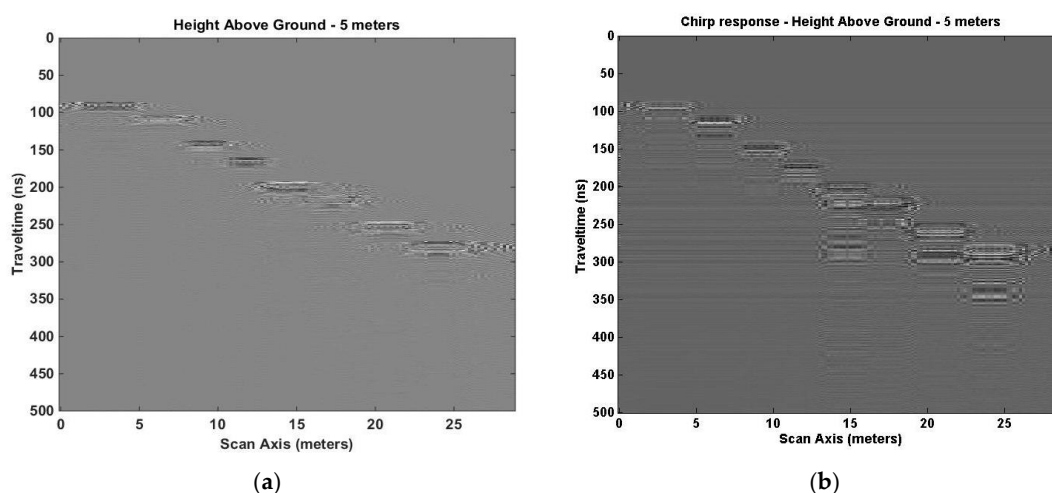


Figure 20. (a) Output response of SA3, EM sum of frequency signals with direct arrival and ground bounce signals removed with Tx/Rx pair 5 m above ground [5]. (b) Output response of SA3 model, chirp excitation function with the direct arrival and ground bounce signals removed with Tx/Rx pair 5 m above ground.

6. Conclusions

In this paper, we explored the idea that perhaps a chirp excitation function could replace the six frequency GPR scans combined using the EM GMM method reported earlier in references [1–5]. This idea was bolstered by Section 2 (related work) discussions on chirp signals in SAR [9–11] systems and ground-based methods, such as vibroseis [12–15], where Gazdaq migration and

compression techniques enhanced chirp received signals. In reviewing EM compositing methods using maximum-likelihood techniques, we determined that the path to better detection was strengthened by the number of times an area was scanned to collect enough data for compositing of signals. We used six frequencies in our earlier studies encompassing a broad range of frequencies (20, 30, 50, 100, 500, and 900 MHz) to image a broad range of targets at different depths. The task we set out to accomplish was to create a chirp excitation signal to replace these six frequencies using the previously defined analysis spaces, media and buried targets.

To that end, we created a linearly increasing chirp excitation signal starting at 20 MHz and ending at 900 MHz. The chirp signal was designed to match each time step created by the previous EM GMM analyses corresponding to the Δx and Δy grid space for a defined model area containing buried targets. The chirp pulse was applied only $\frac{1}{4}$ of the length of time for a single scan to allow for fewer interference reflections from the area being scanned. This length of time is similar to the Ricker pulse excitation function. The Ricker function equation is such that as time increases the magnitude decreases after its maximum value is reached. Using the software program GprMax [6], we repeated the same analyses, previously run with the six individual frequencies, with the generated chirp signal data. The EM GMM method and chirp method results were compared side by side for heights 5, 10, 20, and 40 m, for the same buried targets and media types. The chirp-based GPR response was processed in the same manner as the EM GMM signals; the direct arrival and ground bounce signals were removed before processing further. For the EM GMM case, compositing occurred then the image was plotted. For the chirp case, just the image was plotted. The end product (GPR image plot) was better than we expected for the chirp excitation method but not as good as the EM GMM method. We found that although the edge detection capability of the end product was greatly improved by the chirped response signal, the depth indication was broader. This result was repeated when we added the six frequencies without searching for the best weighted combination; something the EM GMM process does routinely. We found this time and previously that the EM GMM method performed edge protection very poorly, but depth detection very well; very little “ghosting” occurred [1–5].

Taking a page from the SAR processing notebook, we decided to explore the result of correlating the chirp output response with the chirp input signal. This normally produces a better signal-to-noise ratio for the received signal, clearing up noise related problems. That outcome (noise reduction) occurred where multiple lines above the designated target position were significantly reduced but the broad depth indication remained. We implemented Gazdaq [17] migration with the thought that we had a phase shift problem. The result was less effective than the correlation process. The indication was that our 2-D analysis did not have a phase-shift problem.

We repeated chirp, Gazdaq [17], and correlation processes on a more complicated defined space with the same results. We further performed the chirp process on a non-homogenous media defined space, producing the same outcome with some signal degradation due to non-homogenous media interfaces. The EM GMM method remained the superior method, though it would require more passes over an object to achieve good target detection. We showed that, unless one needed the increased resolution, just a chirp excitation signal was good enough to get a coarse idea of the location of buried targets. We concluded, from actual plots, that as the target depth increased, no new information was discovered, so those records were not included in this paper (depths greater than 20 m for SA1 defined space and 10 m for SA2 and SA3 defined spaces).

Problem areas remaining to be addressed are better edge detection techniques, removal of direct wave and ground bounce signals, and how to best align GPR trace starting points across frequencies being used for compositing. We speculate that solving this alignment problem just might reduce the thickness in depth of the scan results. For removal of direct wave and ground bounce we ran each analysis with buried targets in place, then ran the same analysis without the buried targets in place, subtracting the two runs, producing the result we used for further processing.

Author Contributions: Conceptualization, R.T., H.R.S., and F.D.; data curation, formal analysis, investigation, methodology, project administration, resources, software, validation, visualization, writing—original draft, writing—review and editing, R.T.; supervision, H.R.S. and F.D.

Funding: This research received no external funding.

Acknowledgments: This work was performed under the auspices of Sandia National Laboratories, a multimission laboratory managed and operated by National Technology and Engineering Solutions of Sandia, LLC, a wholly owned subsidiary of Honeywell International, Inc. for the U.S. Department of Energy's National Nuclear Security Administration under contract DE-NA-0003525. This paper describes objective technical results and analysis. Any subjective views or opinions that might be expressed in the paper do not necessarily represent the views of the U.S. Department of Energy or the United States Government.

Conflicts of Interest: The authors declare no conflicts of interest.

Appendix A

Appendix A.1 Computer Modeling Verification

To verify that computer modeling could substitute for actual GPR scans, a set of objects were buried at different depths in soil then scanned with a GPR radar, recording the result. The actual test site was located near Greenville, California in the northern Sierra mountains about 60 miles north of Lake Tahoe, California. The tests site was referred to by the name "The Forest Lodge". The objects buried were eight metal (tin) roofing sheets approximately 2 m long by 66 cm by 1.27 mm thick (in depth). The eight sheets were buried individually at depths of 0.5 m, 1 m, 1.5 m, 2 m, 2.75 m, 3 m, 3.5 m, and 4 m, roughly 2 m apart. The soil content appeared to be a mixture of clay and sand, typical for the area. A multi-static radar by MALA GeoScience Corporation was used to perform the GPR scan. The MALA Imaging Radar System (MIRA) consisted of nine transmitters and eight receivers, constructed such that each receiver collected signals from two adjacent transmitters at different times, providing two channels received by one receiver. The structure containing the transmitters and receivers, on wheels, is located about 0.15 m above the ground. The radar provided 16 channels of data covering a 2-m-wide swath over the scan area at a center frequency of 200 MHz, creating a 3-D image. Figure A1 shows the target area with objects in the process of being buried. Figure A2 shows a 3-D plot of the GPR result. Only five of the eight roofing sheets are shown clearly [1,4].



Figure A1. Target ground penetrating radar (GPR) imaging objects, tin roofing sheets, were buried at various depths. The experiments provided ground truth GPR data for hardware to software comparison [1,4].

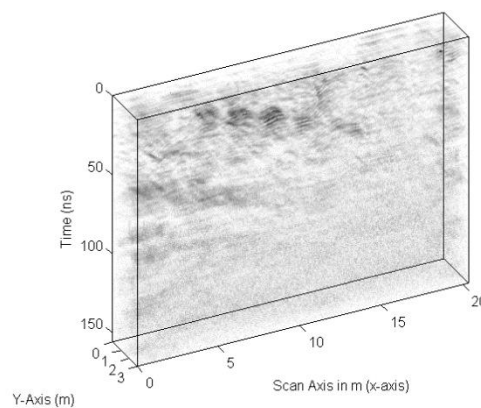


Figure A2. Processed MALA Imaging Radar System (MIRA) radar data over the Forest Lodge test site. Five of the eight buried tin roofing sheets are visible in a stair-step fashion [1,4].

A 3-D model simulating the scan area was constructed with eight sheets buried in a stair-step fashion, 2 m apart, in moist sand, using a GPR software modeling program named GprMax [8]. Figure A3 depicts the GprMax model of the “Forest Lodge” test site with a 0.15-m air gap representing the wheels on the MIRA radar. Figure A4 shows the simulated analysis result for 2-D slices of the 3-D model with direct arrival and ground bounce signals shown. One slice at receiver two and another at receiver six, two of the eight receivers modeled at 200 MHz. All eight simulated buried sheets are visible. The direct arrival (direct path from transmitter to receiver) and ground bounce (reflection path from transmitter to free-space/ground boundary to receiver) signals are displayed prominently at approximately 5 ns. These results strengthen the argument that software analysis can be substituted for hardware and field work. The analysis can be adjusted to better fit the actual output by using a mixture of clay and sand in the model, adjusting the permittivity and conductivity of the medium. These parameters affect the velocity through the medium and the signal attenuation, respectively [1,4].

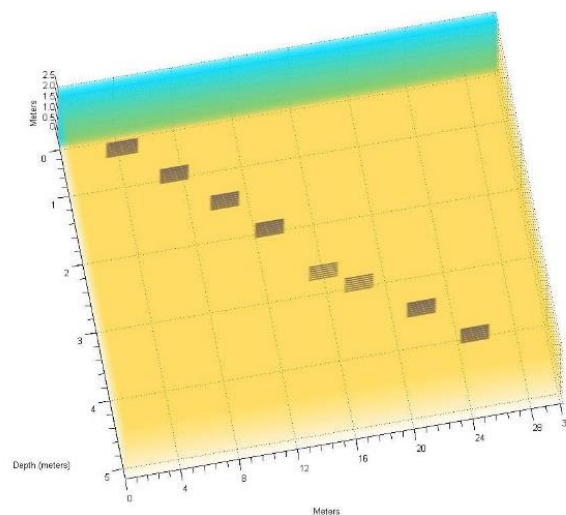


Figure A3. GprMax 3-D model of the Forest Lodge site with eight tin roofing sheets buried objects buried in moist sand including a 0.15-m air space above ground [1,4].

A 2-D model of the “Forest Lodge” site was constructed to increase our knowledge of using GprMax software [8] as a modeling tool. The result of the 2-D analysis performed at 25 MHz and 900 MHz is depicted in Figure A5. At 900 MHz, the position of each plate is well defined. The unexpected results are the “ghost” reflections underneath each plate, reduced as the buried depth of plates increases. At 25 MHz the object detail is minimal, as expected, showing an envelope of all buried roofing sheets. Both scans show the direct arrival and ground bounce signals as expected.

The two-way travel time calculation for signal scans typically begins at the first arrival pulse of the generating excitation function. For low frequencies there is some time (ns) before the generating pulse first arrival response is received thus accounting for the delay in calculating the start of the two-way travel time calculation, shown in the 25 MHz analysis plot. At higher frequencies (above 100 MHz) this delay is very short, often negligible, shown in the 900 MHz plot [1,4].

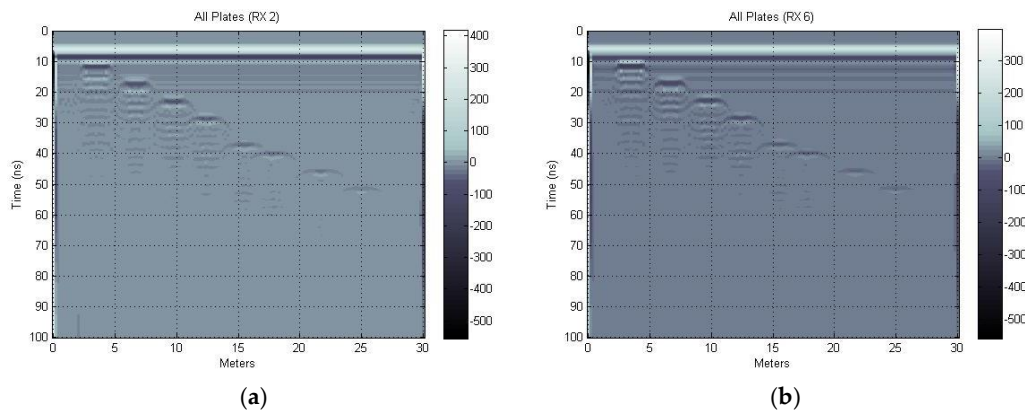


Figure A4. (a) slice Rx 2; (b) slice Rx 6; GPR results at 200 MHz for two 2-D slices of the 3-D analysis results. All eight of the simulated buried tin sheets are shown [1,4].

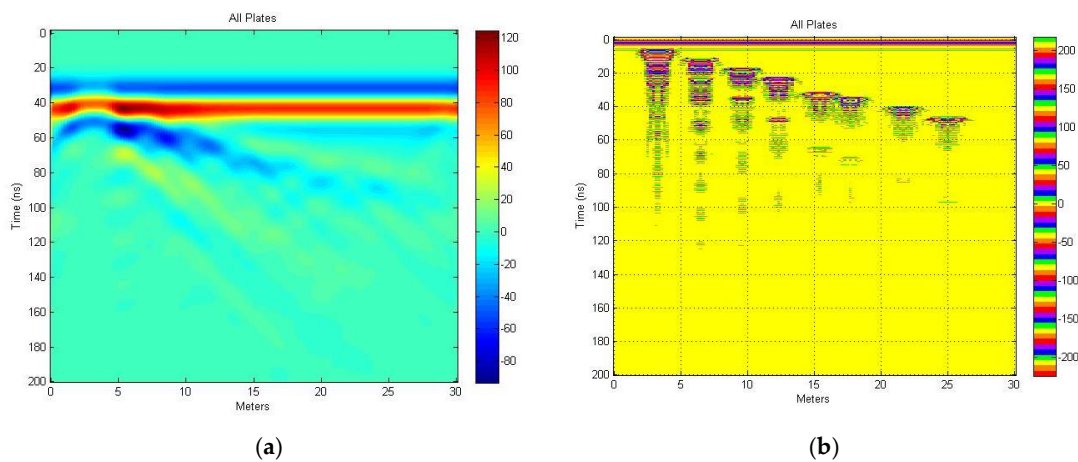


Figure A5. Finite-difference time-domain (FDTD) analysis results of the 2-D model using GprMax at 25 MHz (a) and 900 MHz (b) [1].

The success of the computer simulation with GprMax [8] supports its use as an alternative to hardware scans and field work [1,4].

Appendix A.2 Expectation-Maximization Algorithm Test Case

As a test case for examining the EM GMM method, we constructed a series of six sine waves (50, 150, 250, 350, 450, and 550 Hz), noted in Figures A6–A8, which, when weighted properly, sum to the square wave of Figure A9 (labeled desired). As noted in Figure A9 (labeled EM result), the EM GMM method result is not quite a square wave but well on the way. The apparent error can be attributed to the constraints associated with this implementation, specifically, group membership weights, w_{ik} and/or mixture weights, α_k each constrained to sum to one. The weights normally sum to greater than 1 dependent on the number of signals added together. The constructed sine waves are harmonics of the square wave used [2,4].

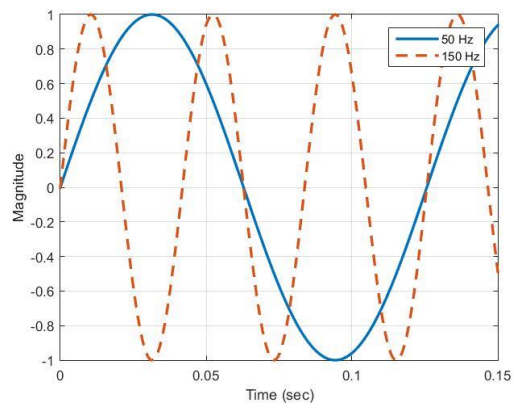


Figure A6. Sine wave frequencies 50–150 Hz [2,4].

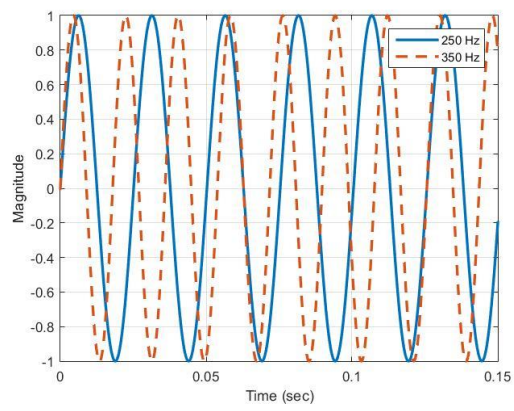


Figure A7. Sine wave frequencies 250, 350 Hz [2,4].

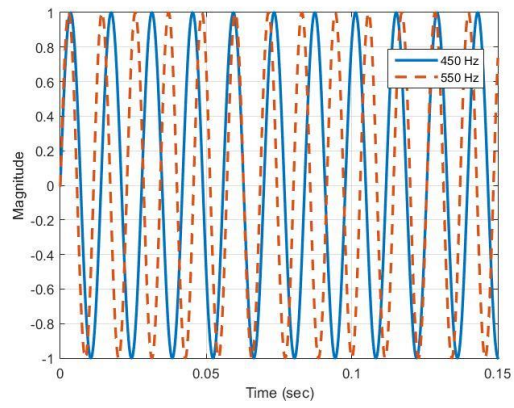


Figure A8. Sine wave frequencies, 450–550 Hz [2,4].

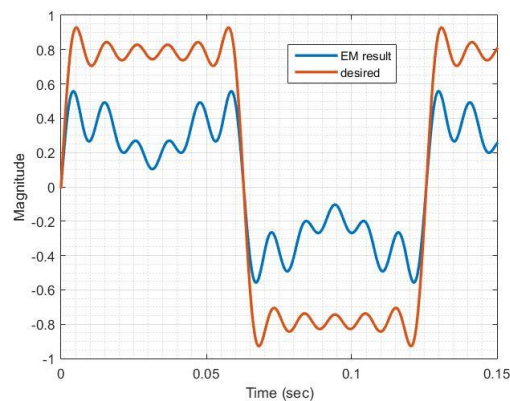


Figure A9. EM GMM Algorithm result; compositing of sinewaves (50, 150, 250, 350, 450, 550 Hz) [2,4].

References

1. Tilley, R.; Dowla, F.; Nekoogar, F.; Sadjadpour, H. GPR Imaging for Deeply Buried Objects: A Comparative Study based on FDTD models and Field Experiments. In Proceedings of the MODSIM World 2011 Conference and Expo, College Park, MD, USA, 3–5 April 2012; pp. 45–51, (NASA/CP-2012-217326), (SEE 20130008625).
2. Tilley, R.; Sadjadpour, H.; Dowla, F. Combining Ground Penetrating Radar Scans of Differing Frequencies Through Signal Processing. In Proceedings of the Ninth International Conference on Advanced Geographic Information Systems, Applications, and Services, GEOProcessing 2017, Nice, France, 19–23 March 2017; pp. 32–38, ISBN 978-1-61208-539-5.
3. Tilley, R.; Sadjadpour, H.; Dowla, F. Extending Ground Penetrating Radar Imaging Capabilities Through Signal Processing. In Proceedings of the 2nd World Congress on Civil, Structural, and Environmental Engineering (CSEE'17), Barcelona, Spain, 2–4 April 2017. [CrossRef]
4. Tilley, R.; Sadjadpour, H.; Dowla, F. Compositing Ground Penetrating Radar Scans of Differing Frequencies for Better Depth Perception. *Int. J. Adv. Softw.* **2017**, *10*, 413–431.
5. Tilley, R.; Sadjadpour, H.; Dowla, F. Compositing ‘Standoff’ Ground Penetrating Radar Scans of Differing Frequencies. *Int. J. Adv. Softw.* **2018**, *11*, under review.
6. Dempster, A.P.; Laird, N.M.; Rubin, D.B. Maximum Likelihood from Incomplete Data via the EM Algorithm. *J. R. Stat. Soc. Ser. B (Methodol.)* **1977**, *39*, 1–38. [CrossRef]
7. Shalizi, C.R. Advanced Data Analysis from an Elementary Point of View. Book Draft from Lecture Notes for Course 36-402 at Carnegie Mellon University, Chapters 19.1–19.2.2, 23 January 2017. Available online: <http://www.stat.cmu.edu/~cshalizi/ADAfaEPoV/ADAfaEPoV.pdf> (accessed on 23 November 2017).
8. Giannopoulos, A. Modelling Ground Penetrating Radar by GprMax. *Constr. Build. Mater.* **2005**, *19*, 755–762. [CrossRef]
9. Chan, Y.K.; Koo, V.C. An Introduction to Synthetic Aperture Radar (SAR). *Prog. Electromagn. Res. B* **2008**, *2*, 27–60. [CrossRef]
10. Allen, C. Synthetic Aperture Radar (SAR) Basics. Course EECS826 University of Kansas Electrical Engineering and Computer Science. Available online: https://people.eecs.ku.edu/~callen58/826/826_SAR_basics-F15.ppt (accessed on 13 February 2019).
11. Moreira, A.; Proats-Iraola, P.; Younis, M.; Krieger, G.; Hajnsek, I.; Papathanassiou, K.P. A tutorial on Synthetic Aperture Radar. *IEEE Geosci. Remote Sens. Mag.* **2013**, *1*, 6–43. [CrossRef]
12. Braile, L. *A Short Course in Seismic Reflection Profiling VI. E. Vibroseis. Earth, Atmospheric, and Planetary Sciences*; Purdue University: West Lafayette, IN, USA, June 2016; Available online: <http://web.ics.purdue.edu/~braile/sage/ShortCourseNotes.6.A.Vibroseis.pdf> (accessed on 17 November 2018).
13. Baeten, G.J.M. Theoretical and Practical Aspects of Vibroseis Method. Ph.D. Dissertation, Delft University of Technology, Department of Mining and Petroleum Engineering, Delft, The Netherlands, 1989. TR diss 1719. Available online: <https://repository.tudelft.nl/islandora/object/uuid:eb96d1ab-38a4-4552-811b-6379409876b5/datastream/OBJ/download> (accessed on 17 November 2018).
14. Lindseth, R. Vibroseis. In *Digital Processing of Geophysical Data—A Review*; Society of Exploration Geophysicists: Calgary, AB, Canada, 1968; Chapter 7; pp. 7.1–7.14. [CrossRef]

15. Veeken, P.; Moerkerken, B. *The Seismic Reflection Method and Its Constraints. Chapter 2, Seismic Stratigraphy and Depositional Facies Models*; Academic Press: New York, NY, USA, 2013; pp. 15, 17–104. [[CrossRef](#)]
16. Stolt, R. Migration by Fourier Transform. *Geophysics* **1978**, *43*, 23–48. [[CrossRef](#)]
17. Gazdag, J. Wave Equation with the phase-shift method. *Geophysics* **1978**, *43*, 1342–1351. [[CrossRef](#)]
18. Holzrichter, M.; Snee, G. Resolution Enhancement of Land Mines in Ground-Penetrating Radar Images. In *Proceedings SPIE 4038, Detection and Remediation Technologies for Mines and Minelike Targets V*; SPIE: Philadelphia, PA, USA, 22 August 2000. [[CrossRef](#)]
19. Özdemir, C.; Demirci, Ş.; Yiğit, E.; Yilmaz, B. A Review on migration Methods in B-Scan Ground Penetrating Radar Imaging. *Math. Probl. Eng.* **2014**, *2014*, 280738. [[CrossRef](#)]
20. Dougherty, M.E.; Michaels, P.; Pelton, J.R.; Liberty, L.M. Enhancement of Ground Penetrating Radar Data Through Signal Processing. In *Proceedings of the Symposium on the Application of Geophysics to Engineering and Environmental Problems*, Boston, MA, USA, 27–31 March 1994; pp. 1021–1028. [[CrossRef](#)]
21. Booth, A.D.; Endres, A.L.; Murray, T. Spectral Bandwidth Enhancement of GPR Profiling Data Using Multiple-Frequency Compositing. *J. Appl. Geophys.* **2009**, *67*, 88–97. [[CrossRef](#)]
22. Endres, A.L.; Booth, A.; Murray, T. Multiple Frequency Compositing of Spatially Coincident GPR Data Sets. In *Proceedings of the Tenth International Conference on Ground Penetrating Radar*, Delft, The Netherlands, 21–24 June 2004; pp. 271–274, ISBN 90-9017959-3.
23. Bancroft, S.W. *Optimizing the Imaging of Multiple Frequency GPR Datasets Using Composite Radargrams: An Example from Santa Rosa Island, Florida*. Ph.D. Dissertation, University of South Florida, Tampa, FL, USA, 2010.



© 2019 by the authors. Licensee MDPI, Basel, Switzerland. This article is an open access article distributed under the terms and conditions of the Creative Commons Attribution (CC BY) license (<http://creativecommons.org/licenses/by/4.0/>).